PSMD14 Drives Clear Cell Renal Cell Carcinoma Progression via JAK/STAT3 Signaling

Wenying Zhang[1,#], Hui Di[1,#], Renpei Xia[2], Jiali Yang[2], Junfeng Zhang[2,*] and Jianyou Gu[2,*]

[1]*Department of Nephrology, The Second Affiliated Hospital of Guangzhou Medical University, Guangzhou 510260, China*

[2]*Institute of Hepatopancreatobiliary Surgery, Chongqing General Hospital, School of Medicine, Chongqing University, Chongqing 401147, China*

Abstract: Cancer hallmarks include senescence, uncontrolled proliferation, and metastasis. We focused on 26S proteasome non-ATPase regulatory subunit 14 (PSMD14), a gene identified from a cellular senescence-related gene signature. We focused on PSMD14, a senescence-associated gene overexpressed in various tumors, to understand its clinical and tumorigenic roles in ccRCC. Based on 279 cellular senescence-related genes collected from the CellAge database, we constructed a prognostic signature for ccRCC patients using TCGA and ArrayExpress datasets. PSMD14 was significantly overexpressed in ccRCC tissues, correlating with malignancy andzidentified as an independent prognostic factor. Single-cell analysis further suggested that PSMD14 expression was associated with malignant cellular phenotypes and activation of the Janus kinase/signal transducer and activator of transcription 3 (JAK/STAT3) signaling pathway. Functional experiments showed PSMD14's role in enhancing ccRCC cell proliferation, migration, and invasion via this pathway. *In vivo*, PSMD14 knockdown significantly reduced tumor growth and JAK/STAT3 pathway activity. Our study positions PSMD14 as a key oncogenic factor in ccRCC, offering a potential therapeutic target.

Keywords: ccRCC, senescence, PSMD14, single-cell, JAK/STAT3.

INTRODUCTION

Renal cell carcinoma (RCC) is one of the most lethal malignant tumors of the urinary system, among which clear cell renal cell carcinoma (ccRCC) accounts for approximately 70-75% of all RCC cases [1-3]. RCC comprises several histologically distinct subtypes, including clear cell RCC, papillary RCC, and chromophobe RCC, each characterized by different pathological features and molecular alterations [4-6]. Among them, ccRCC is distinguished by tumor cells with clear cytoplasm caused by lipid and glycogen accumulation, a rich vascular network, and frequent VHL gene inactivation, which contributes to its unique biological behavior [7-9]. Compared with other RCC subtypes, ccRCC is often associated with higher metastatic potential and poorer clinical outcomes [10,11]. Despite advances in targeted therapy and immunotherapy, the prognosis of patients with advanced ccRCC remains unsatisfactory, largely due to tumor heterogeneity and therapeutic resistance [12,13]. Therefore, identifying reliable prognostic biomarkers and novel therapeutic targets is essential for improving patient stratification and developing individualized precision treatment strategies.

Cellular senescence, defined as a state of permanent cell cycle arrest, is a fundamental biological process involved in aging and tumor development, and targeting senescence-related pathways has emerged as a promising therapeutic strategy for cancer treatment [14-16]. However, the complex link between cellular senescence and cancer, especially ccRCC, remains incompletely understood. As an emerging hallmark of cancer, the relationship between cellular senescence and other malignant biological behaviors of tumors remains unclear. Although senescence plays a protective role in life activities, the accumulation of senescent cells may also promote tumor progression through the secretion of senescence-associated factors during cancer development [17]. On the other hand, cancer aggressiveness is closely related to epithelial mesenchymal transition (EMT), which promotes tumorigenic progression of epithelial cells by increasing cell migration and invasion, and influencing cellular plasticity and apoptosis [18,19]. Therefore, further understanding of the senescence-related molecular programs involved in tumor proliferation and invasion may provide important insights into cancer biology and therapeutic strategies.

26S proteasome non-ATPase regulatory subunit 14 (PSMD14) is included in the CellAge database as a gene associated with cellular senescence [20] and was identified as a key gene within the cellular senescence-related prognostic signature constructed in this study.

*Address correspondence to these authors at the Institute of Hepatopancreatobiliary Surgery, Chongqing General Hospital, School of Medicine, Chongqing University, Chongqing 401147, China;
E-mail: gujianyou5792@163.com, zhangjunfengamu@163.com

#These authors contributed equally.

PSMD14, also known as POH1 or RPN11, has been known as a component of the 19S regulatory particle of the 26S proteasome complex [21-23]. PSMD14 plays an important role in tumor development and progression. Contemporary research indicates that PSMD14 exhibits elevated expression across diverse tumors, encompassing head and neck squamous cell carcinoma, non-small cell lung cancer and esophageal squamous cell carcinoma, and has been reported as an independent prognostic indicator associated with unfavorable outcomes [24-26]. It's broadly acknowledged that PSMD14 has pivotal functions in the proliferation, invasion, migration, stem-like properties, and drug resistance of malignancies such as esophageal squamous cell carcinoma, ovarian cancer, hepatocellular carcinoma, gastric cancer, breast cancer and myeloma [26-33]. However, the diagnostic and prognostic value of PSMD14 and its potential regulatory mechanisms in ccRCC have not been fully understood.

In our current research, we formulated a prognostic risk model based on cellular senescence-related genes to evaluate the prognosis of ccRCC patients. We then further explored the role of PSMD14, a key gene in the model. PSMD14 exhibited elevated expression in ccRCC and may serve as a potential diagnostic and prognostic biomarker. We demonstrated that PSMD14 facilitates proliferation, migration and invasion of ccRCC through activation of the Janus kinase/signal transducer and activator of transcription 3 (JAK/STAT3) signaling pathway *in vitro* and *in vivo*. These findings suggest that PSMD14 plays an important role in the progression of ccRCC. Therefore, targeting PSMD14 may represent a potential therapeutic strategy for ccRCC.

MATERIALS AND METHODS

Data Acquisition and Processing

The gene expression data of ccRCC were downloaded from Gene Expression Omnibus (GEO, including GSE14762, GSE40435, GSE46699, GSE53000, GSE66272 and GSE68417), The Cancer Genome Atlas (TCGA) database and EBI ArrayExpress (accession numbers E-MTAB-1980). Cases with missing prognostic information were excluded from TCGA dataset and E-MTAB-1980 dataset. A total of 531 TCGA-ccRCC samples were split randomly into training (n = 267) and testing (n = 264) cohorts using the CARET package (function createDataPartition) in R. The additional independent dataset, E-MTAB-1980 (n = 101), was enrolled as the validation cohort. The Human Protein Atlas (HPA) database was used to investigate the protein expression level of PSMD14 in ccRCC cancer and normal tissues. We obtained four ccRCC samples (GSM4630028, GSM4630029, GSM5222644, GSM5222645) from the GEO database (GSE152938 and GSE171306) for single-cell level analysis.

Establishment and Validation of the Prognostic Signature Based on Cellular Senescence-Related Genes (CSRS)

We developed a prognostic signature using 279 cell senescence genes from CellAge (https://genomics.senescence.info/cells/). Initially, univariate Cox regression identified prognostic genes ($p < 0.05$, “survival” package) in the training cohort. These genes underwent LASSO regression (“glmnet” package) to reduce overfitting. The optimal shrinkage parameter was determined via 10-fold cross-validation. Subsequently, a risk score model (CSRS) was constructed using multivariate Cox regression. The model's accuracy was evaluated using ROC curves to calculate the AUC. Nomograms were assessed against actual outcomes through calibration charts and the concordance index, using the rms package.

Single-Cell RNA-Seq Analysis Including Dimensionality Reduction, Pseudotime Inference, and Pathway Scoring

Single-cell RNA sequencing (scRNA-seq) data were processed using a standardized pipeline including quality control, normalization, feature selection, and dimensionality reduction. Low-quality cells were filtered based on expression metrics, followed by normalization and identification of highly variable genes. Principal component analysis (PCA) was performed to reduce data dimensionality, and Uniform Manifold Approximation and Projection (UMAP) was subsequently applied to visualize cellular distributions in two-dimensional space. Based on clustering results, differential gene expression analysis was conducted to identify marker genes and characterize cell subpopulations.

To investigate cellular state transitions, pseudotime trajectory analyses were performed using both the CellChat and Monocle 3 packages. CellChat was first used to construct cell–cell communication networks based on ligand–receptor interactions, enabling inference of cell state transitions while incorporating intercellular signaling effects. In parallel, Monocle 3 was used to reconstruct cellular trajectories by

transforming the processed scRNA-seq data into a CellDataSet object, followed by dimensionality reduction, nonlinear embedding, and pseudotime inference to model dynamic cellular changes during disease progression. Visualization and differential gene expression analysis along pseudotime trajectories were further used to identify key genes and biological processes associated with cellular transitions.

To evaluate functional pathway activity at the single-cell level, pathway scoring was performed using the AUCell package. Gene sets associated with cell proliferation, epithelial–mesenchymal transition (EMT), cell migration, JAK/STAT cascade, and IL6/JAK/STAT3 signaling were obtained from the MSigDB database (https://www.gsea-msigdb.org/gsea/index.jsp). AUCell scores were calculated for each cell to quantify pathway activity levels. The resulting pathway scores were visualized using the gg between stats package to compare functional states among different cell populations.

Tissue Microarray (TMA) and Immunohistochemical Analysis (IHC)

TMA comprising 150 ccRCC samples and 30 normal kidney tissues were acquired from Shanghai Outdo Biotech Company. The utilization of tissue samples was authorized by the Ethics Committee of Shanghai Outdo Biotech Company. The IHC procedure was conducted following the guidance provided in the product instruction manual from Maixin, Fuzhou, China.

The IHC scoring system comprehensively considers both the staining intensity and the percentage of cells exhibiting positive staining. Staining intensity is evaluated and graded as follows: 0 (no staining), 1 (weak staining), 2 (moderate staining), and 3 (strong staining). The percentage of positively stained cells is graded as follows: 0 (< 5%), 1 (5% to 25%), 2 (26% to 50%), 3 (51% to 75%), and 4 (> 75%). The staining index (SI) is derived by combining the staining intensity rating with the proportion score of cells showing positive staining. By employing this evaluation technique, tumor specimens are classified into the low expression cohort (SI ≤ 4) and the high expression cohort (SI ≥ 6) concerning the target protein.

Cell Lines and Cell Culture

Two human ccRCC cell lines including Caki-1 and 786-O cells (ATCC, Manassas, VA, USA) were used in this study. The cells were cultured in RPMI 1640 medium (Gibco Invitrogen, Grand Island, NY, USA) supplemented with 10% fetal bovine serum (Gibco Invitrogen, Grand Island, NY, USA) and 1% antibiotic solution, under a controlled environment of 5% CO_2 and 95% ambient air at a temperature of 37℃.

Western Blot

Western blot was performed as previously described [34]. The antibodies used for western blot included those targeting PSMD14 (1:800; Proteintech, USA), p-JAK1 (1:1,000; Cell Signaling Technology, USA), JAK1 (1:1,000; Cell Signaling Technology, USA), p-STAT3 (1:1,000; Cell Signaling Technology, USA), STAT3 (1:1,000; Cell Signaling Technology, USA) and β-actin (1:5,000; Cell Signaling Technology, USA).

Knockdown and Overexpression of PSMD14

PSMD14-specific small interfering RNA (siRNA) and a non-targeting siRNA control were acquired from GenePharma (Shanghai, China). For PSMD14 overexpression, the full-length human PSMD14 gene was integrated into the pEX3 (pGCMV/MCS/Neo) vector, also sourced from GenePharma (Shanghai, China). To establish cell lines with stable PSMD14 knockdown, a PSMD14-targeted short hairpin RNA (shRNA) was incorporated into the pEX-3 (pGCMV/MCS/Neo) vector, enabling shPSMD14 lentivirus production (GenePharma, Shanghai, China). Following this, 786-O cells underwent transduction with the concentrated lentivirus. Transfection was conducted using Lipofectamine 3000 (Invitrogen, Carlsbad, USA), adhering to the prescribed protocol.

Inhibition of the JAK/STAT3 Pathway

To facitinib is a JAK family kinases tyrosine kinase inhibitor that inhibits JAK/STAT3 activation *in vitro* and *in vivo* [35-37]. JAK/STAT3 signal pathway inhibitor Tofacitinib was purchased from MCE (1 μM, Shanghai, China). The ccRCC cells that overexpressed PSMD14 were treated with Tofacitinib (1 μM) for 6 h. Control cells were treated with dimethyl sulfoxide (DMSO). These processed cells were then subjected to subsequent examinations.

Cell Proliferation Analysis

The proliferative capacity of ccRCC cells was assessed using the 5-Ethynyl-2′-deoxyuridine (EdU) immunofluorescence technique as per the guidelines provided by the manufacturer (RiboBio, Guangzhou, China). For the EdU assay, 5×10^4 transfected cells

were seeded into 96-well plates and subsequently subjected to EdU and immunofluorescence staining.

Migration and Invasion Assays

Cell migration and invasion were evaluated using Transwell assays. Briefly, 5 × 10^4 transfected cells were harvested and resuspended in serum-free Dulbecco's Modified Eagle Medium (DMEM), and then seeded into the upper chamber of the Transwell insert. The lower chamber was filled with DMEM supplemented with 10% fetal bovine serum (FBS) as a chemoattractant. After incubation for 24 hours at 37 °C, the cells remaining on the upper surface of the membrane were gently removed with a cotton swab. The cells that had migrated to the lower surface of the membrane were fixed with 4% paraformaldehyde and stained with 0.5% crystal violet. The stained cells were then visualized and counted under a microscope.

For invasion assays, the procedures were performed in a similar manner, except that the Transwell inserts were pre-coated with Matrigel (Merck Millipore, USA) according to the manufacturer's instructions.

Animal Experiments

In this study, female BALB/c nude mice, aged 4-6 weeks, were sourced from the Peking University Animal Center, Beijing, China, to establish PSMD14 knockdown mouse xenograft models. The mice were allocated into two groups, each consisting of five animals. Each group was subjected to a subcutaneous injection of 5×10^6 PSMD14 knockdown 786-O cells or control cells in the axillary region. Tumor dimensions, specifically length (L) and width (W), were meticulously measured on a weekly basis using a digital Vernier caliper. Tumor volume was calculated employing the formula ($L*W^2$)/2. Adhering to ethical guidelines and to prevent undue tumor proliferation, the mice were humanely euthanized at three weeks post-injection. Subsequently, the tumors were excised and weighed for analysis. The protocol for this study was approved by the Ethics Committee of The Second Affiliated Hospital of Guangzhou Medical University.

Statistical Analysis

Statistical evaluations were conducted utilizing GraphPad Prism 9 software (GraphPad Software, San Diego, CA, USA). Results were represented as the average ± standard deviation (SD). Survival distributions were assessed through Kaplan-Meier plots and evaluated with log-rank (Mantel-Cox) tests. For comparative analysis, we employed the Student's t-test (for two sets) or ANOVA coupled with Tukey's post-hoc test (for multiple sets). All comparisons were

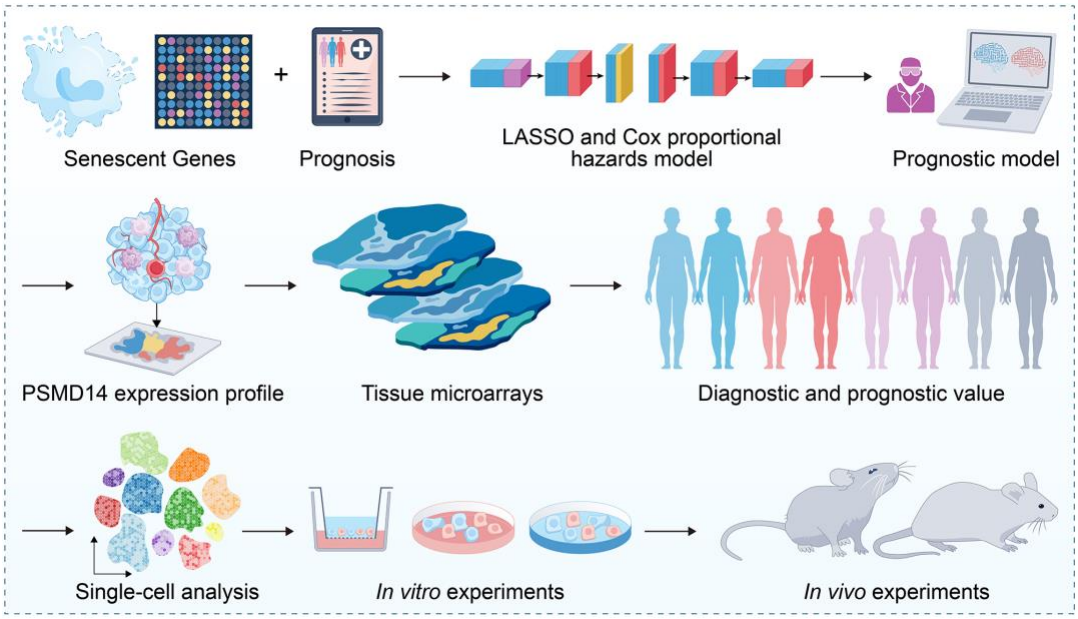

Figure 1: Flow Chart. First, cellular senescence-related genes were collected from the CellAge database and integrated with prognostic information from ccRCC cohorts to construct a senescence-related prognostic model. Prognostic genes were identified using LASSO regression and Cox proportional hazards analysis, and a cellular senescence-related signature was established to evaluate survival risk in patients with ccRCC. Based on this model, PSMD14 was identified as a key gene of interest. Subsequently, public datasets were used to analyze the expression pattern of PSMD14 in ccRCC, and tissue microarray analysis was performed to further validate its expression level and assess its diagnostic and prognostic value. In addition, single-cell RNA sequencing data from public databases, together with *in vitro* and *in vivo* experiments, were integrated to systematically evaluate the functional role and potential molecular mechanisms of PSMD14 in ccRCC.

bi-directional, with a significance threshold set at p < 0.05 (*p < 0.05; **p < 0.01; ***p < 0.001; ****p < 0.0001).

RESULTS

Establishment and Validation of the CSRS in ccRCC

After univariate, Lasso, and multivariate Cox regression analyses, we screened eight cellular senescence-related genes (Figure **1**). Based on these prognostic genes, a CSRS was constructed for ccRCC survival prediction (Figure **2A-C**). The formula for calculating the risk score according to the CSRS was given as follows: risk score = (0.748 * PSMD14) + (0.4361 * VENTX) + (0.2234 * POU5F1) + (0.1498 * KSR2) + (0.1233 * NR2E1) + (0.5457 * SIN3B) + (-0.4539 * YPEL3) + (-0.6469 * MATK). Within the TCGA training set, patients were stratified into either low- or high-risk categories based on the median risk score derived. Those assigned high-risk scores consistently exhibited unfavorable outcomes across the TCGA training set, TCGA validation set, and E-MTAB-1980 validation set (Figure **3A-C**). The Harrell's concordance index (C-index) for the TCGA training set stood at 0.595, while the corresponding values for the validation sets were 0.625 (TCGA) and 0.82 (E-MTAB-1980). To further refine the precision of the CSRS prediction, we employed receiver operating characteristic (ROC)

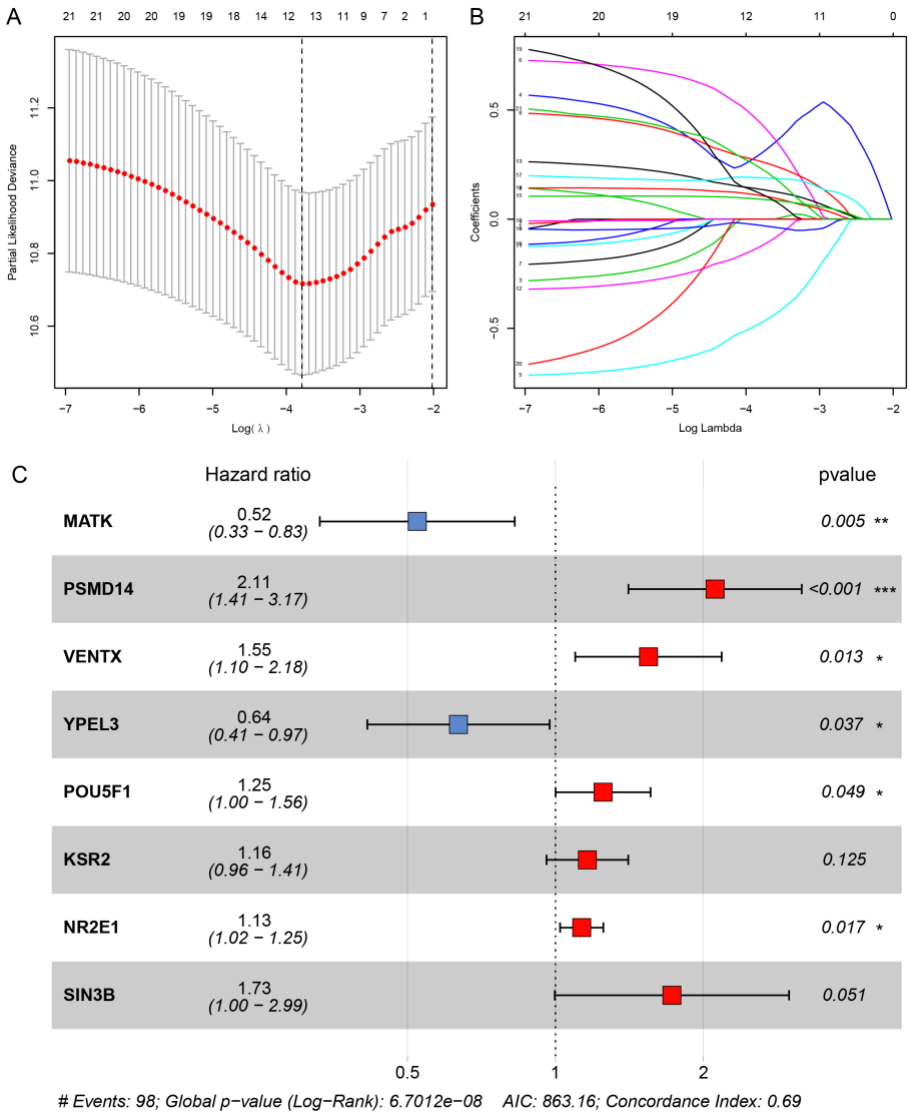

Figure 2: Identification of prognostic cellular senescence-related DEGs. (**A**) The coefficients of candidate genes are shown by lambda parameter. The abscissa represents the value of lambda, and the ordinate represents the coefficients of the independent variable. (**B**) The partial likelihood deviance was plotted against log(λ) using the LASSO model. (**C**) Forest plot of eight cellular senescence-related genes originating from the Cox proportional hazards model. *p < 0.05; **p < 0.01; ***p < 0.001. LASSO, least absolute shrinkage and selection operator.

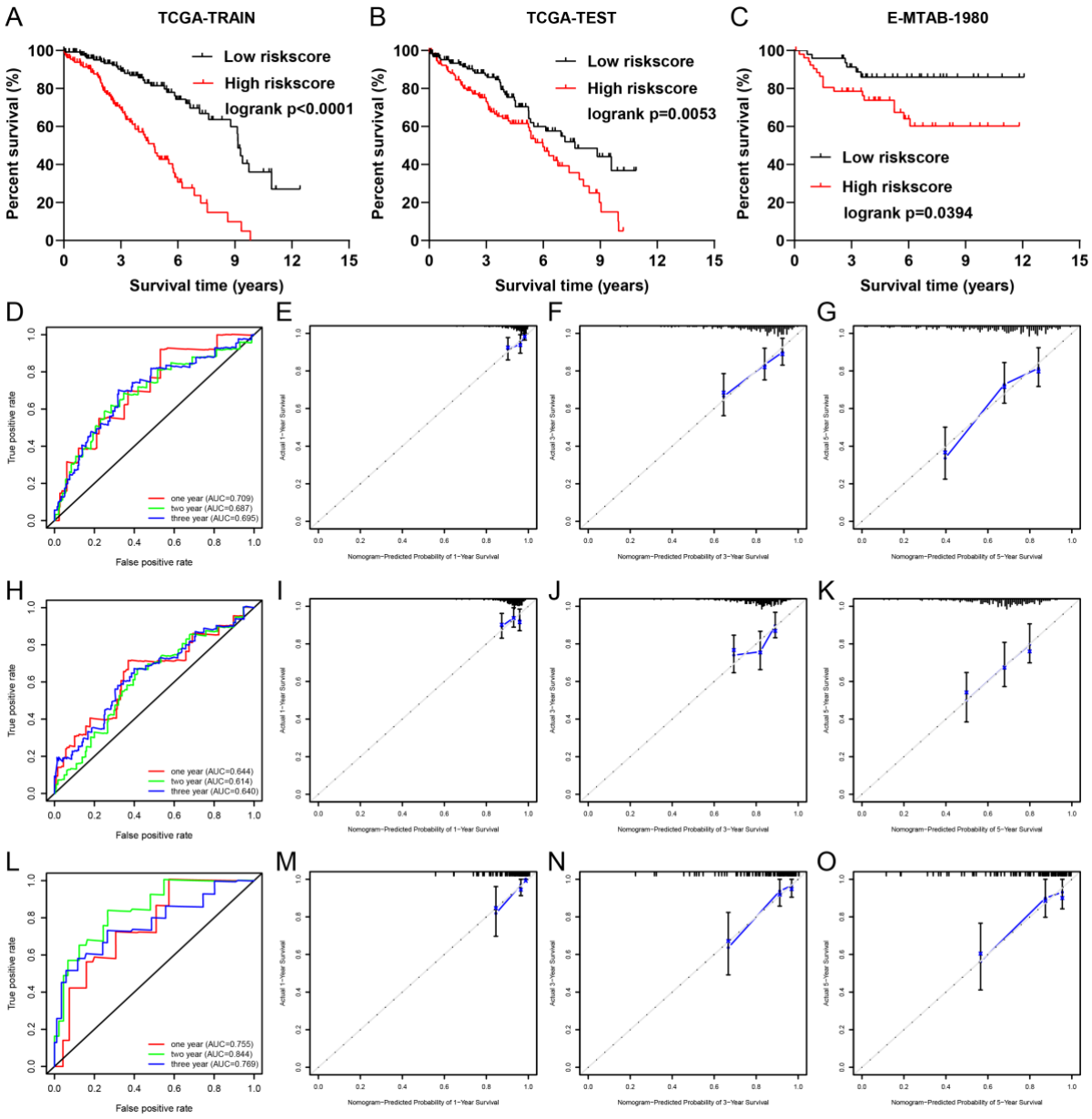

Figure 3: Validation of the CSRS in TCGA and E-MTAB-1980 cohort. (**A-C**) Kaplan-Meier curves for OS in ccRCC patients of TCGA training dataset (**A**), TCGA testing dataset. (**B**) and E-MTAB-1980 dataset (**C**) based on risk score. (**D**, **H** and **L**). Time-dependent ROC curve of the prognostic model for the training set (**D**) and validation set (**H** and **L**). (**E-G**, **I-K** and **M-O**) The calibration curves of the nomogram showed that the nomogram has good calibration capability for the training set (**E-G**; 1, 3 and 5 years), and the calibration curve in the validation set was similar to that of the training set (**I-K** and **M-O**; 1, 3 and 5 years). CSRS, cellular senescence-related signature; ROC, Receiver operating characteristic; AUC, the area under the curve.

curve evaluations, taking the area under the curve (AUC) as an indicator of predictive accuracy. The AUC of the CSRS was 0.695 for the training set and 0.640, 0.769 for the validation set (Figure **3D**, **H**, **L**). In addition, we generated calibration curves to assess the accuracy of the prediction model both in three cohorts and the resulting calibration curves exhibit good linearity in the calibration range (Figure **3E-G**, **I-K** and **M-O**). The nomogram survival prediction model exhibited great feasibility and high accuracy when calculating the ccRCC patients' risk score and predicting the one-year, two-year, three-year, and five-year overall survival probability (Figure **4**). Hence, we developed a prognostic framework centered on genes associated with cellular senescence, offering a precise and user-friendly method to forecast the survival duration of ccRCC patients.

PSMD14 Overexpression in ccRCC Correlates with Poor Prognosis

PSMD14, with the highest weight coefficient (0.748) and hazard ratio (2.11) among eight key genes,

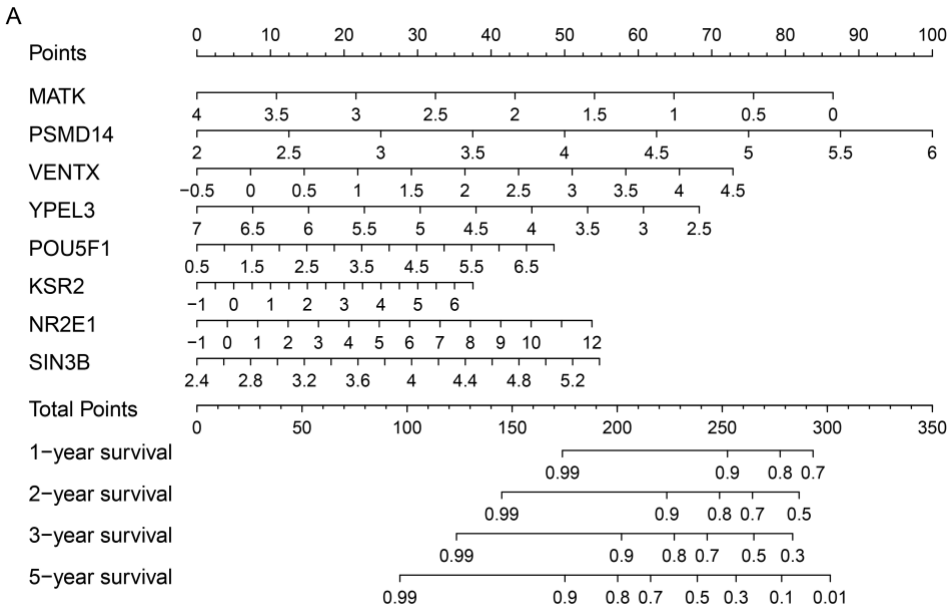

Figure 4: Nomogram of the CSRS. (**A**) The nomogram was established based on the eight genes screened. CSRS, cellular senescence-related signature.

showed significant overexpression in ccRCC tissues versus non-tumor tissues in GEO datasets (GSE14762, GSE40435, GSE46699, GSE53000, GSE66272, GSE68417), as evidenced by mRNA expression profiles and ROC curve analysis (Figure **5A-L**). Kaplan-Meier plots linked high PSMD14 levels to lower overall survival in ccRCC patients (Figure **5M-N**), and staining comparisons highlighted its pronounced expression in ccRCC versus normal tissues (Figure **6A-F**).

Statistical analysis of the TCGA-ccRCC dataset revealed strong associations between PSMD14 expression and clinical parameters (histologic_grade, pathologic_T, N, M, and stage) (Table **1**). Univariate and multivariate Cox proportional hazard evaluations identified PSMD14 as an independent risk factor with significant prognostic value (HR = 1.679, p = 0.001) (Table **2**), underscoring its potential as a standalone prognostic indicator in ccRCC.

PSMD14 is Associated with Malignant Biological Behaviors and JAK/STAT3 Signalling Pathway in ccRCC

Gene Set Enrichment Analysis (GSEA) across multiple datasets (GSE14762, GSE40435, GSE46699, GSE53000, GSE66272, GSE68417, TCGA, E-MTAB-1980) revealed PSMD14's association with EMT and regulation of ccRCC via the JAK/STAT3 pathway (Figure **7A-H**). Gene Set Variation Analysis (GSVA) analysis showed a positive correlation between PSMD14 expression and tumor proliferation in TCGA-ccRCC data (Figure **7I**).

Next, we analyzed the impact and potential molecular mechanisms of PSMD14 on ccRCC tumor cell functions using single-cell RNA sequencing data. Firstly, UMAP dimensionality reduction analysis was performed on 4 ccRCC samples, revealing distinct clusters of subpopulations, with tumor cells forming a separate cluster (Figure **8A**). Cell communication analysis revealed close interactions between tumor cells and other cell types, primarily mediated by molecules such as MIF, VEGFA, SPP1, and VEGFB (Figure **8B**). Subsequently, tumor cells were isolated and divided into high and low PSMD14 expression groups. The high PSMD14 expression group showed significantly higher scores in CELL PROLIFERATION ($p<0.001$, Figure **8C**), EMT ($p<0.001$, Figure **7D**), and CELL MIGRATION ($p<0.001$, Figure **7E**), indicating that tumor cells with high PSMD14 expression exhibit higher proliferative, migratory, and epithelial-to-mesenchymal transition capabilities compared to those with low PSMD14 expression, indicating higher malignancy. Further analysis of the potential mechanisms underlying the effects of PSMD14 on the malignant behaviors of ccRCC tumor cells revealed significantly higher scores in JAK/STAT CASCADE ($p<0.001$, Figure **8F**) and IL 6/JAK/STAT3 SIGNALING ($p<0.001$, Figure **7G**) in the high PSMD14 expression group, suggesting that PSMD14 may promote tumor cell malignant progression through the activation of the JAK/STAT3 pathway. Pseudotime analysis indicated that as tumor cells progressed, the expression trends of PSMD14 and key molecules (JAK1 and STAT3) in the JAK/STAT3 pathway were consistent, providing

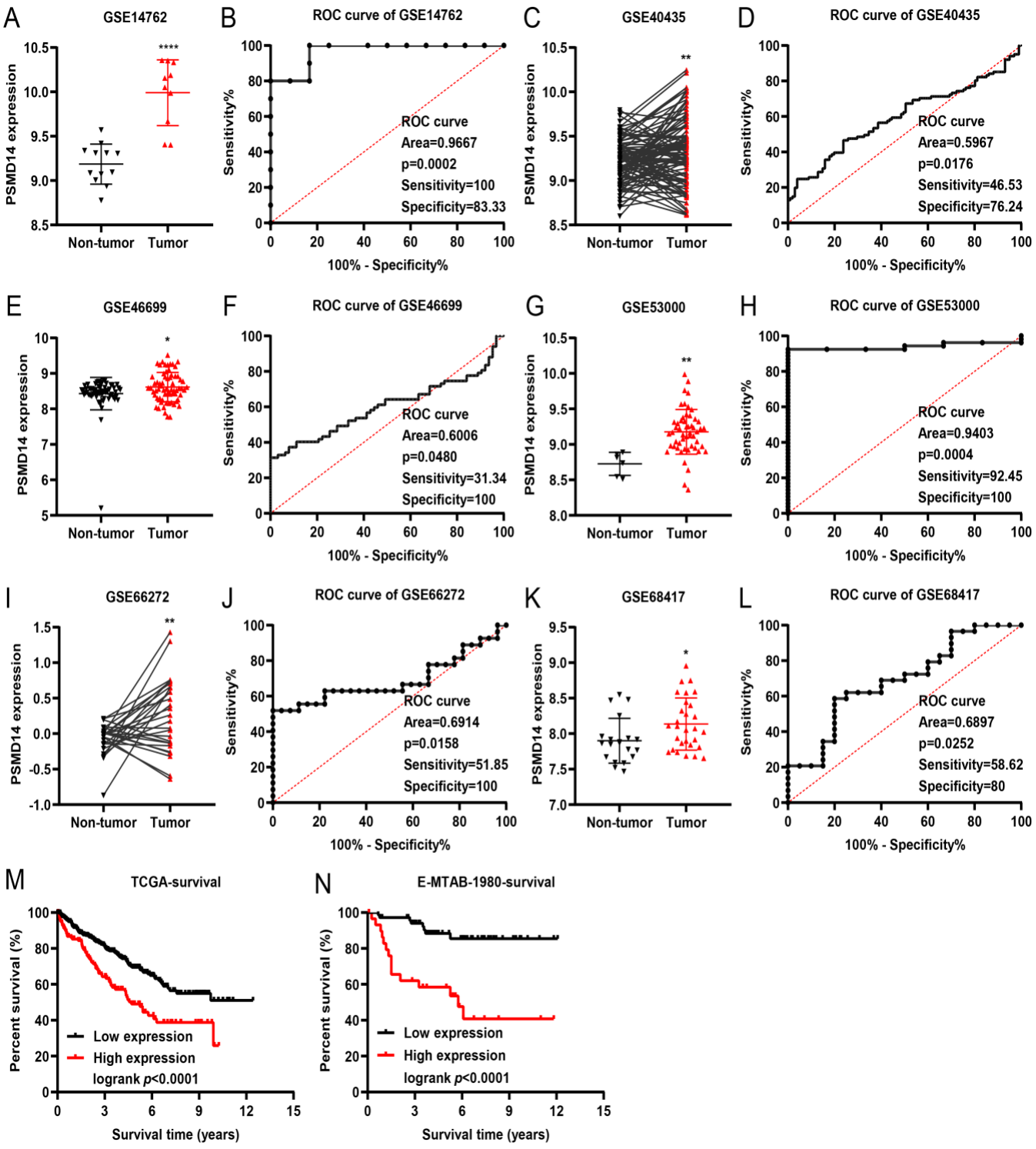

Figure 5: PSMD14 is highly expressed in ccRCC and associated with poor prognosis. (A-L) The mRNAs expression profile of PSMD14 and corresponding ROC curves in ccRCC patients were obtained from the public database (GSE14762, GSE40435, GSE46699, GSE53000, GSE66272 and GSE68417). GSE40435 and GSE66272 contain paired tumor and adjacent normal tissues and are presented with paired lines connecting matched samples, whereas GSE14762, GSE46699, GSE53000, and GSE68417 consist of independent (unpaired) tumor and normal samples, which are displayed as individual data points. (M-N) Kaplan-Meier analysis of overall survival in ccRCC patients with low and high PSMD14 expression. *p < 0.05, **p < 0.01, ***p < 0.001, ****p < 0.0001. ROC, receiver operating characteristic; IHC, immunohistochemical.

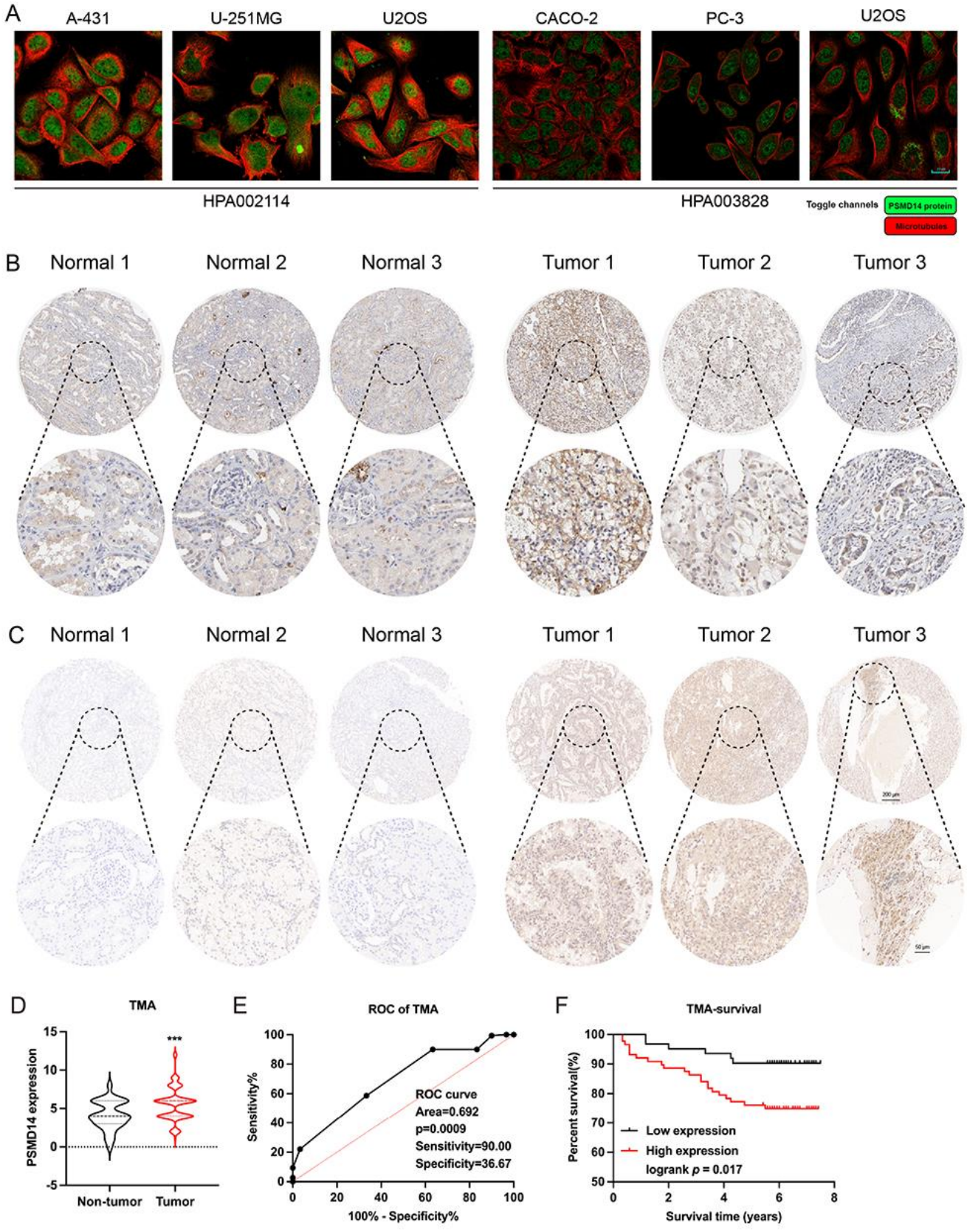

Figure 6: PSMD14 is associated with poor prognosis. (**A**) The subcellular localization of PSMD14 from HPA. (**B-C**) Representative IHC staining of PSMD14 protein in ccRCC tumor and normal tissues obtained from HPA dataset (**B**) and TMA (**C**). (**D-E**) The protein expression level of PSMD14 and corresponding ROC curves in ccRCC TMA cohort patients. (**F**) Kaplan-Meier analysis of overall survival in ccRCC TMA cohort patients with low and high PSMD14 expression. ***p < 0.001. TMA, tissue microarray; ROC, receiver operating characteristic; IHC, immunohistochemical.

Table 1: Clinical Characteristics of Kidney Clear Cell Carcinoma Stratified according to PSMD14 Expression

Characteristics	Low group (n = 388)	High group (n = 143)	p-value
Age (years)			
< 60	183 (47.2%)	65 (45.5%)	0.801
>= 60	205 (52.8%)	78 (54.5%)	
Gender			
female	128 (33.0%)	55 (38.5%)	0.283
male	260 (67.0%)	88 (61.5%)	
histologic_grade			
well differentiated	12 (3.1%)	1 (0.7%)	<0.001
moderately differentiated	184 (47.4%)	46 (32.2%)	
poorly differentiated	152 (39.2%)	54 (37.8%)	
undifferentiated	35 (9.0%)	39 (27.3%)	
unknown	5 (1.3%)	3 (2.1%)	
pathologic_T			
T1	218 (56.2%)	53 (37.1%)	<0.001
T2	46 (11.9%)	24 (16.8%)	
T3	121 (31.2%)	58 (40.6%)	
T4	3 (0.8%)	8 (5.6%)	
pathologic_N			
N0	172 (44.3%)	67 (46.9%)	<0.001
N1	5 (1.3%)	11 (7.7%)	
unknown	211 (54.4%)	65 (45.5%)	
pathologic_M			
M0	318 (82.0%)	104 (72.7%)	0.04
M1	48 (12.4%)	30 (21.0%)	
unknown	22 (5.7%)	9 (6.3%)	
stage			
stage i	214 (55.2%)	51 (35.7%)	0.002
stage ii	38 (9.8%)	20 (14.0%)	
stage iii	84 (21.6%)	39 (27.3%)	
stage iv	50 (12.9%)	32 (22.4%)	
unknown	2 (0.5%)	1 (0.7%)	

Table 2: Cox Univariable and Multivariable Analysis of Clinicopathological Variables and PSMD14 Expression in Relation to OS in Kidney Clear Cell Carcinoma Patients

Clinical factor	Univariable analysis			Multivariable analysis		
	HR	95%CI	p-value	HR	95%CI	p-value
Age (>=60 vs. <60 years)	1.810	1.32-2.481	< 0.001	1.642	1.193-2.259	0.002
Gender (male vs. female)	0.934	0.684-1.276	0.669			
histologic_grade (VS. undifferentiated)				-	-	-
poorly differentiated	0.375	0.264-0.533	< 0.001			
moderately differentiated	0.196	0.131-0.293	＜0.001			
well differentiated	< 0.001	0-＜0.001	0.939			
unknown	0.151	0.021-1.09	0.061			
pathologic_T (VS. T1)				-	-	-
T2	1.593	0.952-2.665	0.076			
T3	3.440	2.422-4.887	< 0.001			
T4	10.927	5.505-21.692	< 0.001			
pathologic_N (VS. N0)				-	-	-
N1	3.492	1.856-6.568	< 0.001			
unknown	0.809	0.593-1.103	0.180			
pathologic_M (VS. M0)				-	-	-
M1	4.413	3.225-6.037	< 0.001			
unknown	0.785	0.248-2.481	0.680			
stage (VS. stage i)						
stage ii	1.280	0.687-2.386	0.436	1.203	0.643-2.248	0.563
stage iii	2.786	1.844-4.207	< 0.001	2.437	1.606-3.698	< 0.001
stage iv	6.890	4.676-10.153	< 0.001	6.193	4.191-9.152	< 0.001
unknown	7.631	1.039-56.029	0.046	8.669	1.177-63.828	0.034
PSMD14 expression (High vs. Low)	1.901	1.396-2.589	< 0.001	1.679	1.226-2.299	0.001
OS, overall survival; HR, hazard ratio						

further evidence that PSMD14 may promote tumor progression by activating the JAK/STAT3 pathway (Figure **8H-J**).

Silencing Of PSMD14 Inhibited Ccrcc Cell Proliferation, Migration, And Invasion

We utilized Caki-1 and 786-O cell lines with PSMD14 knockdown and overexpression to investigate its role in ccRCC. EdU assays revealed that PSMD14 knockdown significantly inhibited cancer cell proliferation (Figure **9A-C**). Wound healing and Transwell migration assays confirmed a marked reduction in cell migration (Figure **9D-F**), while Matrigel invasion assays showed a substantial decrease in the invasive capabilities of ccRCC cells following PSMD14 knockdown (Figure **9G-H**, **I-J**).

Overexpression of PSMD14 Promoted Ccrcc Cells Proliferation, Migration and Invasion

Also, in Caki-1 and 786-O cells, we overexpressed PSMD14 to verify its biological function. Through a battery of tests encompassing EdU, wound healing,

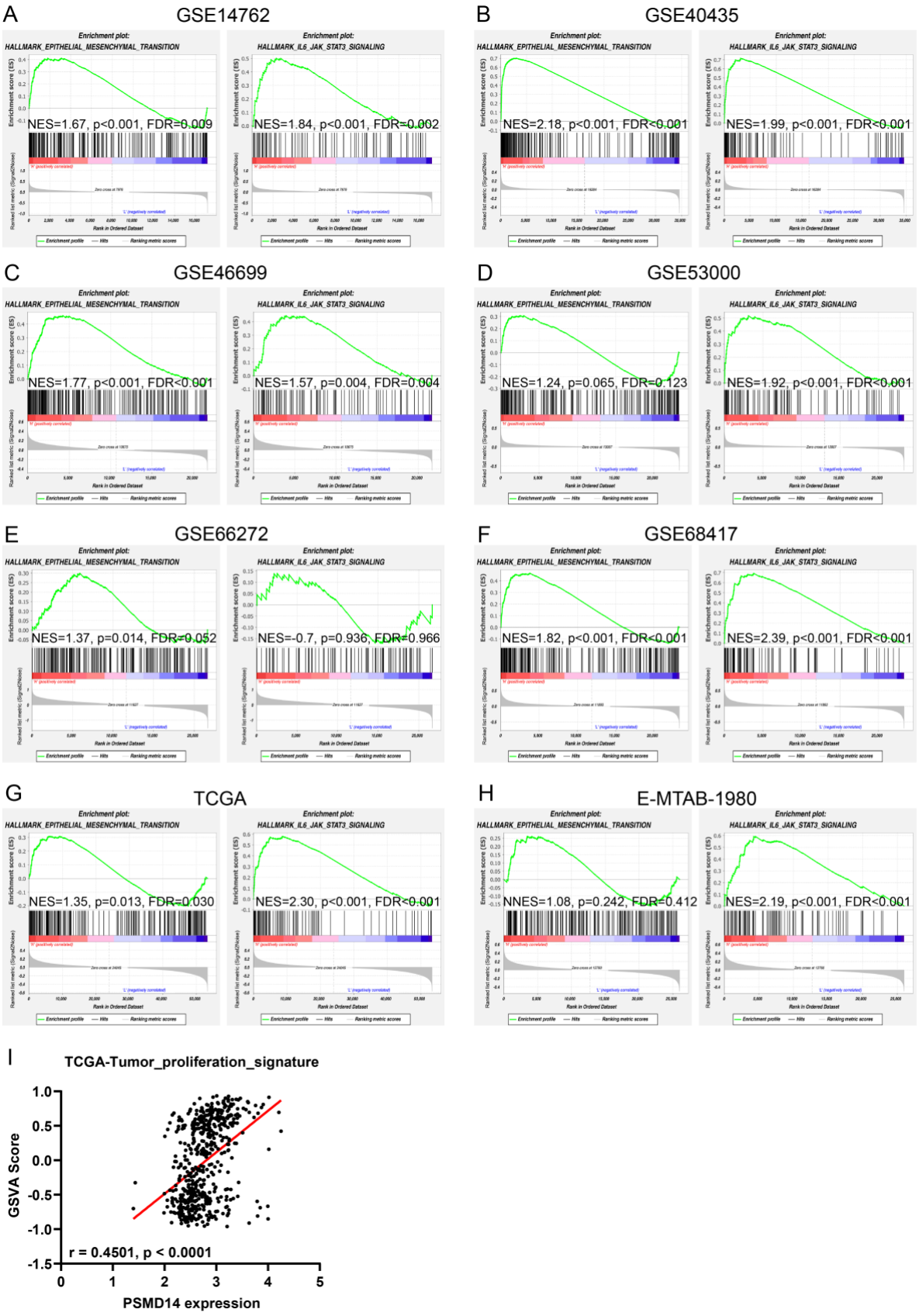

Figure 7: PSMD14 promoted the EMT and JAK/STAT3 signaling pathway in ccRCC. (**A-H**) GSEA indicated that PSMD14 mRNA expression level from public datasets in ccRCC was positively correlated with EMT and JAK/STAT3 pathway. (I) PSMD14 expression was positively associated with tumor proliferation signature using GSVA method.

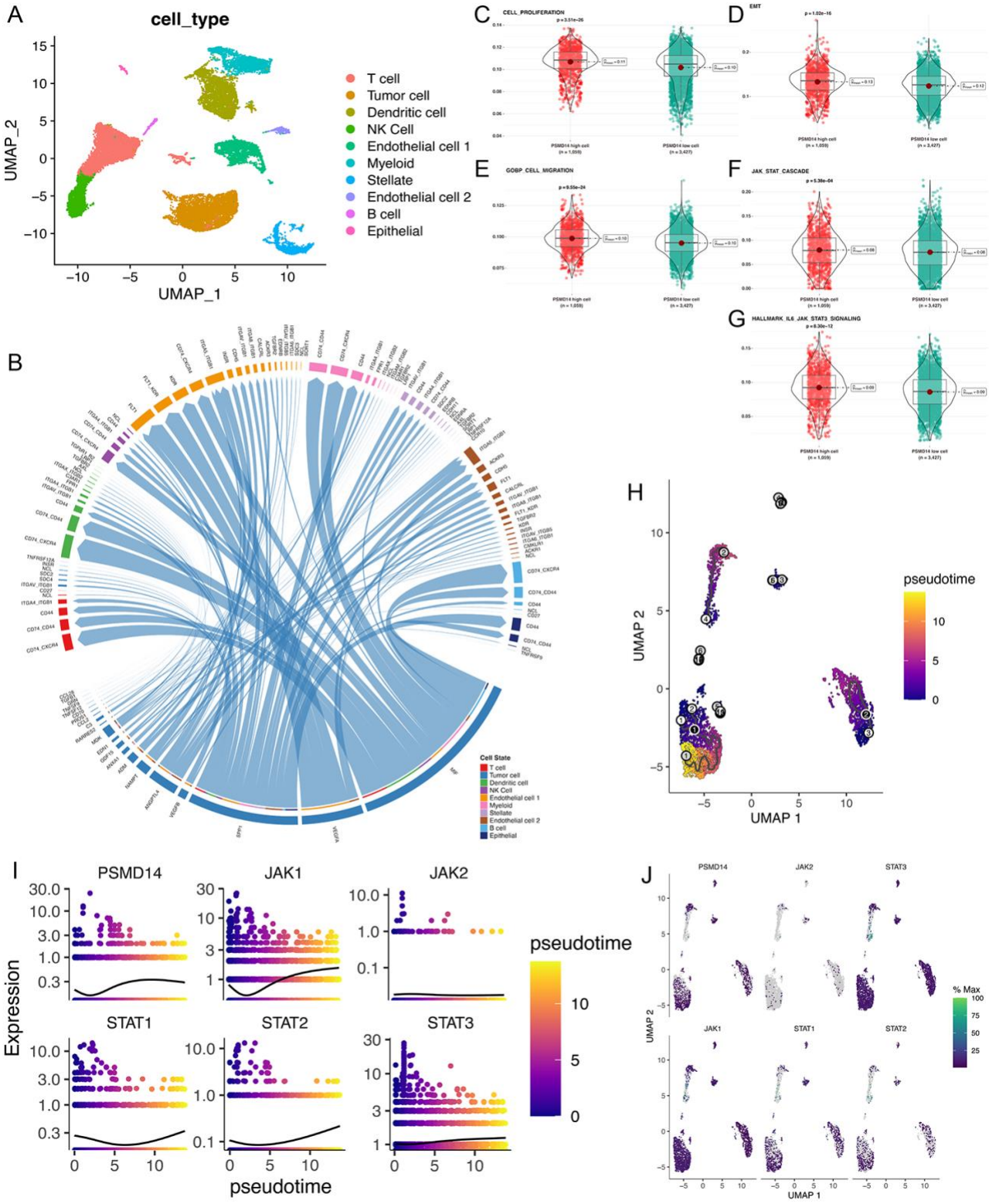

Figure 8: Unveiling the correlation of PSMD14 with the malignant behaviors of ccRCC and the JAK/STAT3 signaling pathway at the single-cell level. (**A**) UMAP dimensionality reduction analysis of 4 ccRCC samples from GSE152938 and GSE171306 datasets based on cell types. (**B**) Cell communication analysis between tumor cells and other cell types. (**C**) Differential CELL PROLIFERATION scores in tumor cells between the high and low PSMD14 expression groups. (**D**) Differential EMT scores in tumor cells between the high and low PSMD14 expression groups. (**E**) Differential GOBP CELL MIGRATION scores in tumor cells between the high and low PSMD14 expression groups. (**F**) Differential JAK STAT CASCADE scores in tumor cells between the high and low PSMD14 expression groups. (**G**) Differential HALLMARK IL6/JAK/STAT3 SIGNALING scores in tumor cells between the high and low PSMD14 expression groups. (**H**) Pseudotime analysis of tumor cells in ccRCC single-cell sequencing samples. (**I**) Trends of gene expression change along the pseudotime. (**J**) Expression patterns of genes in different pseudotime subgroups.

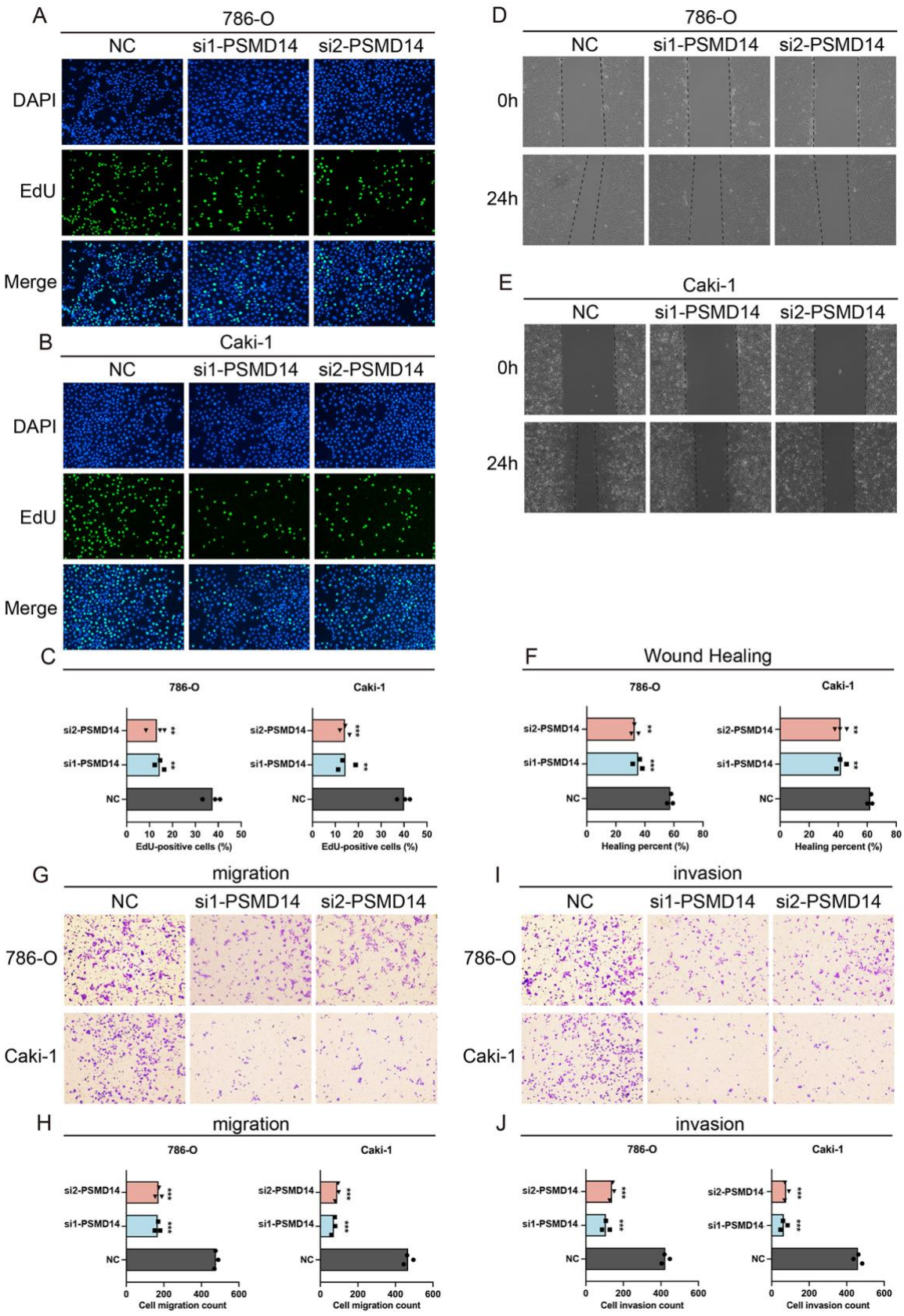

Figure 9: Silencing of PSMD14 inhibited ccRCC cells proliferation, migration and invasion. (**A-D**) EdU assays revealed that PSMD14 knockdown inhibited proliferation in Caki-1 and 786-O cells. (**E-F** and **I**) Wound healing assays showed that PSMD14 knockdown reduced migrating capacity of the indicated cells. (**G-H** and **J-K**) Transwell migration assays (**G**, **J**) and matrigel invasion assays (**H**, **K**) confirmed that PSMD14 knockdown dramatically decreased the migrating capacity and invading ability of ccRCC cells. One-way ANOVA was followed by Tukey's multiple comparison tests. *P < 0.05; **P < 0.01; ***P < 0.001.

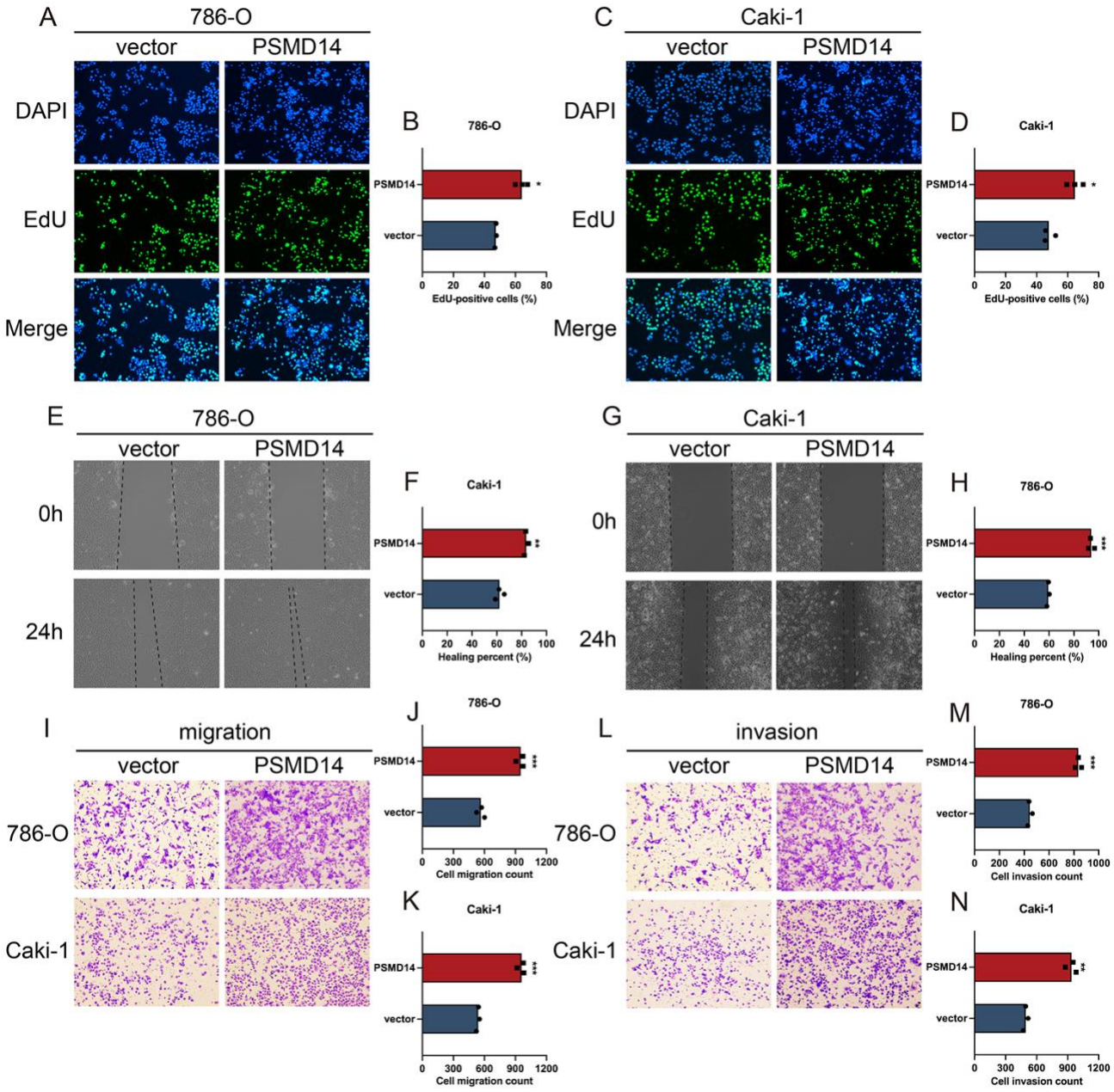

Figure 10: Overexpression of PSMD14 promoted ccRCC cells proliferation, migration and invasion. (**A-C**) EdU assays revealed that PSMD14 overexpression promoted proliferation in Caki-1 and 786-O cells. (**D-F**) Wound healing assays showed that PSMD14 overexpression induced migrating capacity of the indicated cells. (**G-J**) Transwell migration assays (**G-H**) and Matrigel invasion assays (**J-J**) confirmed that PSMD14 knockdown dramatically increased the migrating capacity and invading ability of ccRCC cells. Student's t-test. *P < 0.05; **P < 0.01; ***P < 0.001.

Transwell migration, and Matrigel invasion assays, it was evident that, in contrast to the loss-of-function experiment, an upregulation of PSMD14 enhanced the proliferative, migratory, and invasive capabilities of ccRCC cells (Figure **10A-N**).

The JAK/STAT3 Signaling Pathway is Essential for PSMD14-induced Malignant Behaviors of Cancer Cells

GSEA and single-cell analyses indicated a positive correlation between PSMD14 and the JAK/STAT3 pathway (Figures **6A-H**, Figure **8G-J**). Cell lines with PSMD14 overexpression were treated with the JAK inhibitor Tofacitinib, with cells transfected with empty vector and DMSO as controls. Post-treatment, Tofacitinib reversed PSMD14-induced proliferation, migration, and invasion (Figure **11**). Western blotting showed decreased p-JAK1 and p-STAT3 in PSMD14 knockdown cells and increased levels in overexpressing cells (Figures **12A-B**). Tofacitinib counteracted the upregulation of p-JAK1 and p-STAT3 caused by PSMD14 overexpression (Figure **12C**).

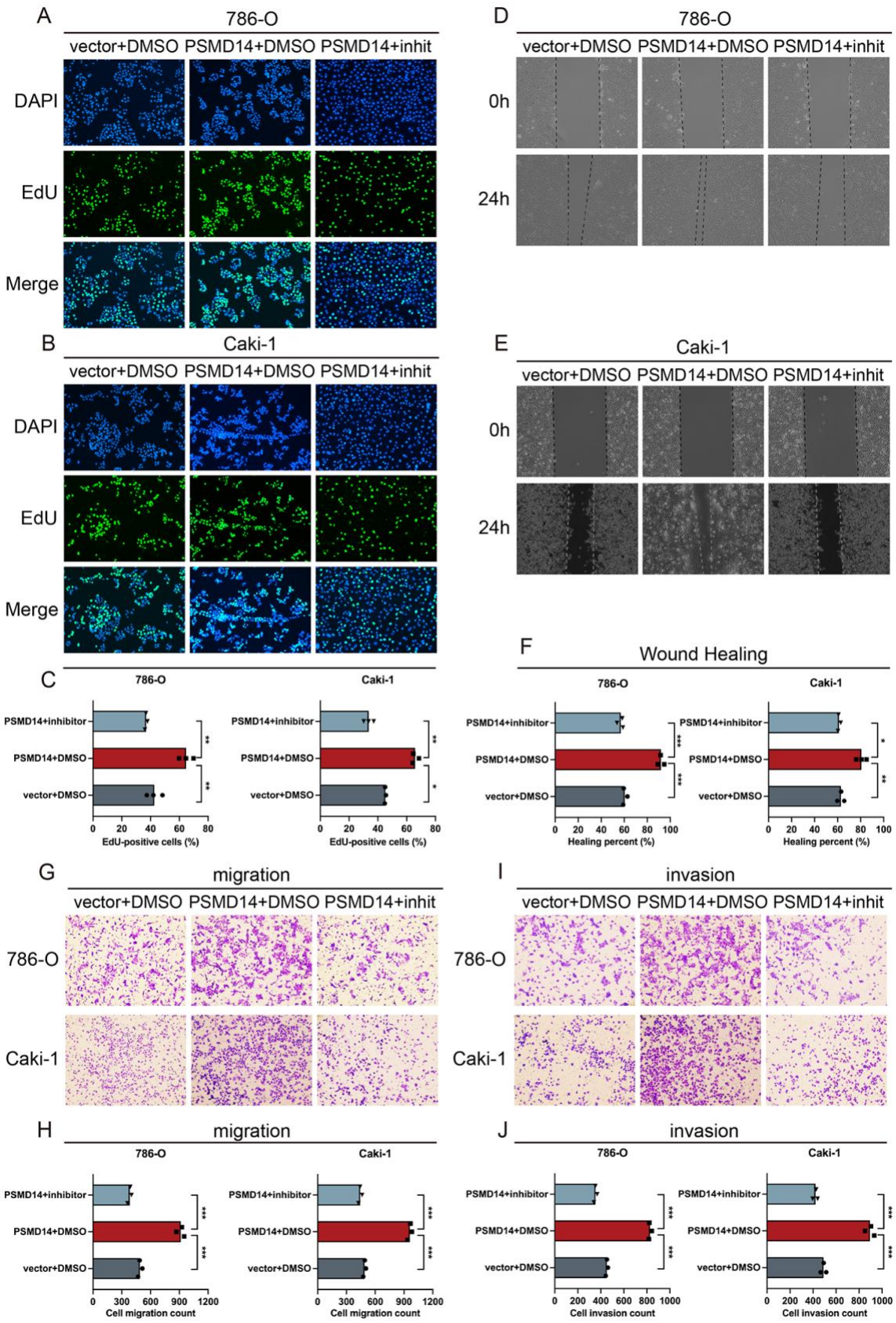

Figure 11: The JAK/STAT3 signaling pathway is essential for PSMD14-induced malignant behaviors of cancer cells. (**A-D**) Representative micrographs of EdU staining and corresponding quantifications of Caki-1 and 786-O cells. (**E-H**) The wound healing process was measured by scratch wound healing assay at 0 and 24 hours. (**I-N**) Migration and invasion abilities were evaluated using transwell migration (**I-K**) and Matrigel invasion assays (**L-N**). One-way ANOVA was followed by Tukey's multiple comparison tests. *P < 0.05; **P < 0.01; ***P < 0.001.

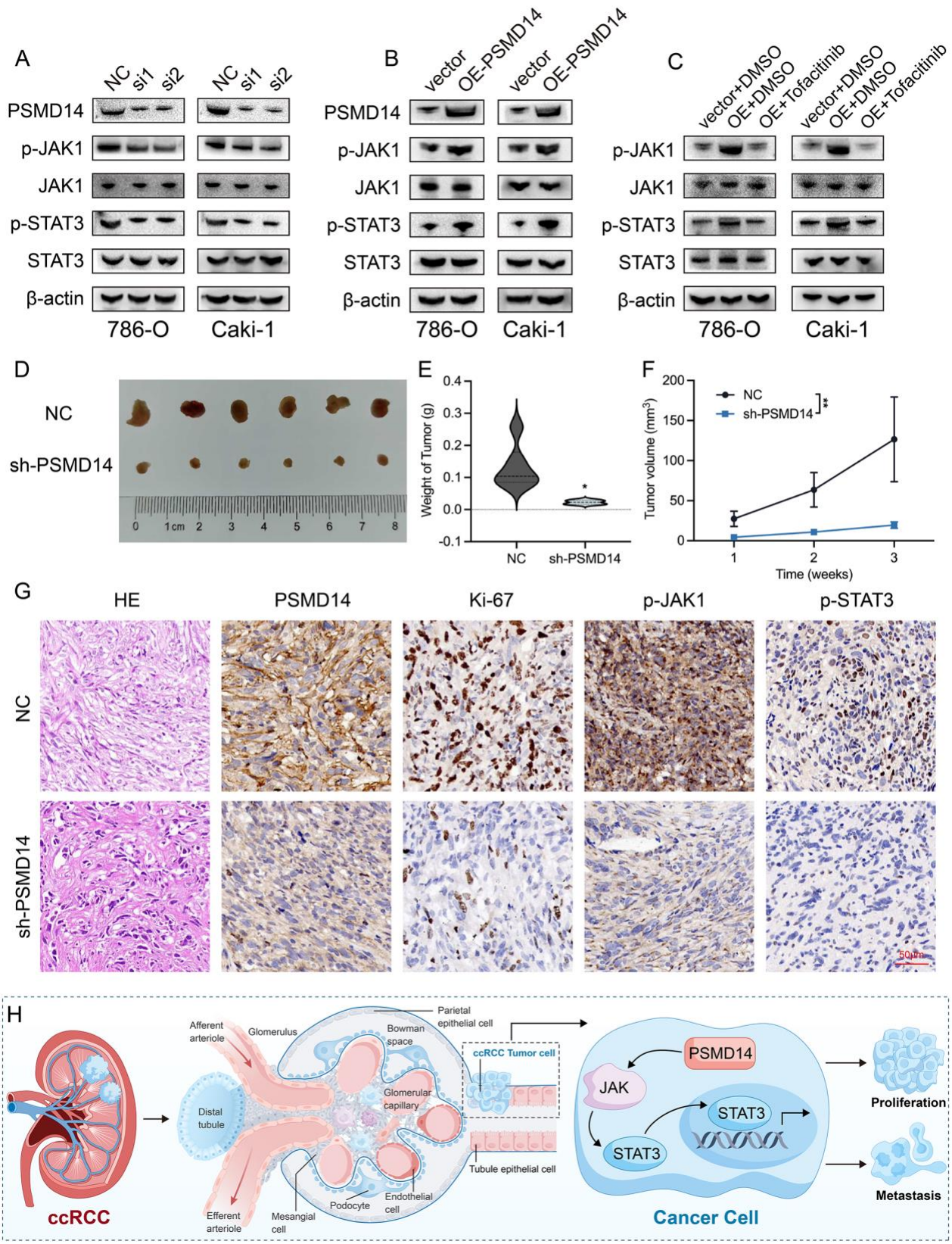

Figure 12: The PSMD14/JAK/STAT3 axis promoted malignant behaviors of ccRCC. (**A-C**) Western blotting on the expression of PSMD14, phosphorylated-JAK1, total JAK1, phosphorylated-STAT3 and total STAT3 in the indicated cells. β-actin was the loading control. (**D**) Representative xenograft images from selected mouse cohorts. (**E**) Average tumor weight. (**F**) Tumor volume measurements on predetermined dates. (**G**) Hematoxylin-eosin (**HE**) and immunohistochemical analyses of tumor specimens. (**H**) Schematic illustration of potential mechanisms of PSMD14/JAK/STAT3 axis accelerated malignant behaviors of ccRCC. *P < 0.05; **P < 0.01.

These findings confirm PSMD14's influence on cell proliferation, migration, and invasion via the JAK/STAT3 pathway.

PSMD14 Augments Malignancy in ccRCC *in vivo*

To elucidate the *in vivo* biological impact of PSMD14, a subcutaneous xenograft model using nude mice was developed. Observations indicated that PSMD14 knockdown markedly diminished both the weight and volume of these xenografts (Figure **12D-F**). IHC analysis of the xenograft tissues indicated a reduction in the expression levels of Ki-67, p-JAK1, and STAT3 following PSMD14 knockdown (Figure **12G**). These findings imply that PSMD14 could enhance malignant characteristics in ccRCC, potentially driving tumor progression via the JAK/STAT3 signaling pathway (Figure **12H**).

DISCUSSION

In our research, we devised the CSRS framework, offering a reliable prognostic prediction for ccRCC patients. Within this model, PSMD14 stands out as a pivotal gene, exhibiting marked overexpression in ccRCC. Patients with elevated PSMD14 levels face unfavorable outcomes. Functional assays further underscored PSMD14's role in augmenting ccRCC cell proliferation, migration, and invasion. Moreover, PSMD14 exerts its cancer-promoting functions through JAK/STAT3 signaling pathway.

Cellular senescence stands as a defining feature of aging, and the build-up of these senescent cells within human tissues is perceived as a predisposing element for age-associated ailments, including cancer [38-40]. Some researchers have used senescence-related genes to construct models to predict the prognosis of patients, and have shown outstanding performance [41]. In this study, we constructed a prognostic signature based on cellular senescence-related genes and identified PSMD14 as a key gene within this model, which had a reliable performance in predicting patient prognosis. According to this signature, scores were calculated for ccRCC patients, and patients with high CSRS score had poor prognosis. However, how senescent cells adversely affect cancer patients and how they interact with other tumor hallmarks such as proliferation, invasion, and migration has not been reported, especially in ccRCC cancer. To further explore the biological significance of this model, we selected PSMD14, a key gene within the CSRS, for further functional investigation.

It is an urgent pursuit of oncologists to find accurate and efficient independent prognostic factors. PSMD14 has been reported to be highly expressed in a variety of tumors such as head and neck squamous cell carcinoma and non-small cell lung cancer and can be used as an independent predictor of poor prognosis [24,25]. Accumulating evidence suggests that aging-associated molecular programs, together with metabolic adaptations, chromatin dynamics, and evolving resistance networks, cooperatively drive tumor aggressiveness and treatment failure across multiple cancer types [42-46]. However, the prognostic value of PSMD14 has not been investigated in ccRCC. In GEO and HPA databases, PSMD14 is highly expressed in ccRCC tumor tissues compared with normal tissues. In TCGA, E-MTAB-1980 datasets and our tissue-microarray cohort, patients with high PSMD14 expression had a shorter survival time. These results are similar to previous studies, which suggested that PSMD14 could be an independent prognostic factor for ccRCC.

Abnormal and uncontrolled cell proliferation, activating invasion and metastasis are hallmarks of cancer [47]. As the functional executor of biological behaviors, some key proteins regulate these tumor-promoting behaviors [48-55]. PSMD14 is a 19S-proteasome-associated deubiquitinating enzyme and has been reported that PSMD14 has multiple oncogenic effects in various cancers. In ovarian cancer, hepatocellular carcinoma, esophageal squamous cell carcinoma, and breast cancer, PSMD14 promotes cell proliferation, invasion, and migration [29,31,32,56]. The present study demonstrated that PSMD14 overexpression remarkedly promoted the proliferation, migration, and invasion of ccRCC cells by single-cell analysis, EdU, CCK8 and Transwell assays. These results suggest that PSMD14 may act as a novel oncogene in ccRCC and may be a potential therapeutic target.

The JAK/STAT3 signaling pathway has been implicated in many cancers, where it has been shown to promote tumor growth and progression by contributing to cellular transformation [57,58]. In this study, we performed GSEA after dividing PSMD14 expression into high and low groups in several public datasets, and the results all suggested that PSMD14 was positively correlated with JAK/STAT3 signaling pathway. Moreover, single-cell analysis revealed that the PSMD14 high-expression group was positively correlated with the JAK/STAT3 signaling pathway

score. Rescue experiments after the treatment of pathway inhibitors confirmed that PSMD14 played a role in regulating the malignant behavior of ccRCC through the JAK/STAT3 signaling pathway. Moreover, our *in vivo* experiments revealed that the ablation of PSMD14 led to the suppression of tumor malignancy and the JAK/STAT3 pathway. However, the study has reported that PSMD14 regulates chemoresistance of head and neck squamous cell carcinoma through E2F1/Akt/ SOx2 mediated stemness [30]. In hepatocellular carcinoma, deubiquitinase PSMD14 promotes cancer growth and metastasis by stabilizing GRB2 [31]. In the meantime, PSMD14 contributes to hyperactivation of TGF-β signaling and accelerates hepatocellular carcinoma metastasis through deubiquitinating TGF-β receptors and caveolin-1 [59]. Our study revealed tumor heterogeneity and enriched the molecular mechanism by which PSMD14 regulates the development and progression of ccRCC. However, this study has several limitations that should be acknowledged. First, the association between PSMD14 and cellular senescence was mainly derived from bioinformatic identification within a senescence-related gene signature rather than direct experimental validation. Although PSMD14 was selected from this model, the present work primarily demonstrates its functional role in promoting ccRCC proliferation, migration, and invasion through the JAK/STAT3 signaling pathway. Second, the single-cell RNA sequencing analysis was performed on a relatively small number of samples, which may limit the generalizability of the single-cell level observations. Third, although multiple public datasets and experimental approaches were used to support our findings, further studies with larger cohorts and additional mechanistic experiments are needed to validate these results. Further studies will be required to determine whether PSMD14 directly participates in regulating cellular senescence in ccRCC.

CONCLUSION

Our study constructed and validated a cellular senescence-related signature based on eight cellular senescence-related genes that have important prognostic significance for ccRCC patients. Importantly, we explored the role of PSMD14, a key gene in the signature, in promoting tumor proliferation, migration and invasion via JAK/STAT3 signaling pathways in ccRCC. Our results indicate that PSMD14 protein could serve as a prognostic marker and a potential therapeutic target for ccRCC treatment.

ETHICS APPROVAL AND CONSENT TO PARTICIPATE

Tissue Microarray was acquired from Shanghai Outdo Biotech Company. The utilization of tissue samples was authorized by the Ethics Committee of Shanghai Outdo Biotech Company. The animal experiment was approved by the Ethics Committee of The Second Affiliated Hospital of Guangzhou Medical University.

COMPETING INTERESTS

The authors declare no conflict of interest.

FUNDING

This work was supported by Guangdong Medical Science and Technology Research Fund (No. A2025241) and Plan on enhancing scientific research in GMU for Wenying Zhang; Natural Science Foundation of Chongqing, China (No. CSTB2024NSCQ-MSX1113) for Renpei Xia.

AUTHORS' CONTRIBUTIONS

Wenying Zhang and Hui Di contributed to conception, design and data analysis of the study. Renpei Xia, Jiali Yang contributed to acquisition of data and technical support. Junfeng Zhang and Jianyou Gu helped write and revise the manuscript. All authors read and approved the final manuscript.

ACKNOWLEDGEMENTS

Not applicable.

REFERENCES

[1] Wang J, Nan Y, Liu Q, Ding T, Liu D, Duo L, *et al*. Tumor-Resident Streptococcus pneumoniae Promotes Malignant Progression and Pazopanib Resistance in Clear Cell Renal Cell Carcinoma. Cancer Res 2026. https://doi.org/10.1158/0008-5472.CAN-25-3780

[2] Abu-Remaileh M, Stransky LA, Bhalerao N, Shirole NH, Jiang Q, Saad E, *et al*. Targeting of HIF2-driven cachexia in kidney cancer. Nat Med 2026; 32(1): 245-257. https://doi.org/10.1038/s41591-025-04054-2

[3] Yue N, Zhao H, Zhang Y, Gu J, Qi J, Wen J, *et al*. Lysophosphatidylethanolamine 18: 1 drives clear cell renal cell carcinoma by stabilizing SIRT6 to reprogram lipid metabolism. Signal Transduct Target Ther 2025; 10(1): 398. https://doi.org/10.1038/s41392-025-02496-1

[4] Xu Y, Shen Y, Zhang C, Zheng L, Ji F, Chen J, *et al*. Exploring the Effect of Fidgetin-Like 1 on Colorectal Cancer Through Tissue Chip and In vitro Experiments. Balkan Med J 2024; 41(6): 491-498. https://doi.org/10.4274/balkanmedj.galenos.2024.2024-7-9

[5] Elias R, Nirschl T, Rezaee M, Yerrapragada A, Wang S, Cheaib J, *et al*. Clear-Cell Renal Cell Carcinoma Molecular Subtypes Differ by African and European Genetic Similarity. Cancer Res Commun 2025; 5(5): 743-755. https://doi.org/10.1158/2767-9764.CRC-24-0624

[6] Jiang Q, Braun DA, Clauser KR, Ramesh V, Shirole NH, Duke-Cohan JE, *et al*. HIF regulates multiple translated endogenous retroviruses: Implications for cancer immunotherapy. Cell 2025; 188(7): 1807-1827.e1834. https://doi.org/10.1016/j.cell.2025.01.046

[7] Shirole NH, Kesar D, Lee Y, Goodale A, Syamala S, Kukreja S, *et al*. Requirement for Cyclin D1 Underlies Cell-Autonomous HIF2 Dependence in Kidney Cancer. Cancer Discov 2025; 15(7): 1484-1504. https://doi.org/10.1158/2159-8290.CD-24-1378

[8] Dawidek MT, Calderon LP, Shah PK, Mittal R, Ucpinar BA, Bakouny Z, *et al*. MLH1 Mismatch Repair Deficiency Predicts Exceptional Response to Immune Checkpoint Inhibition in Clear-cell Renal Cell Carcinoma. Eur Urol 2025. https://doi.org/10.1016/j.eururo.2025.09.4162

[9] Huang B, Ren J, Ma Q, Yang F, Pan X, Zhang Y, *et al*. A novel peptide PDHK1-241aa encoded by circPDHK1 promotes ccRCC progression via interacting with PPP1CA to inhibit AKT dephosphorylation and activate the AKT-mTOR signaling pathway. Mol Cancer 2024; 23(1): 34. https://doi.org/10.1186/s12943-024-01940-0

[10] Hahn AW, Chahoud J, Skelton WP, Yuan Y, Zurita-Saavedra AJ, Kovitz C, *et al*. A multicenter randomized phase II trial of lenvatinib plus everolimus versus cabozantinib in patients with metastatic clear-cell RCC that progressed on PD-1 immune checkpoint inhibition (LenCabo). Ann Oncol 2026; 37(2): 241-249. https://doi.org/10.1016/j.annonc.2025.10.009

[11] Deng Q, Ji Y, Liu J, Wen T. Lipid reprogramming and ferroptosis crosstalk in clear cell renal cell carcinoma: metabolic vulnerabilities and therapeutic targeting. Mol Cancer 2025; 24(1): 236. https://doi.org/10.1186/s12943-025-02457-w

[12] Lombardi O, Li R, Jabbar F, Evans H, Halim S, Lima J, *et al*. Conserved patterns of transcriptional dysregulation, heterogeneity, and cell states in clear cell kidney cancer. Cell Rep 2025; 44(1): 115169. https://doi.org/10.1016/j.celrep.2024.115169

[13] Ge Q, Meng J, Wang Z, Anwaier A, Lu J, Tian X, *et al*. Spatially segregated APOE(+) macrophages restrict immunotherapy efficacy in clear cell renal cell carcinoma. Theranostics 2025; 15(11): 5312-5336. https://doi.org/10.7150/thno.109097

[14] Geng L, Ping J, Wu R, Yan H, Zhang H, Zhuang Y, *et al*. Systematic profiling reveals betaine as an exercise mimetic for geroprotection. Cell 2025; 188(19): 5403-5425.e5433. https://doi.org/10.1016/j.cell.2025.06.001

[15] Lei J, Xin Z, Liu N, Ning T, Jing Y, Qiao Y, *et al*. Senescence-resistant human mesenchymal progenitor cells counter aging in primates. Cell 2025; 188(18): 5039-5061.e5035. https://doi.org/10.1016/j.cell.2025.05.021

[16] Wu Z, Qu J, Liu GH. Roles of chromatin and genome instability in cellular senescence and their relevance to ageing and related diseases. Nat Rev Mol Cell Biol 2024; 25(12): 979-1000. https://doi.org/10.1038/s41580-024-00775-3

[17] Omer A, Barrera MC, Moran JL, Lian XJ, Di Marco S, Beausejour C, *et al*. G3BP1 controls the senescence-associated secretome and its impact on cancer progression. Nat Commun 2020; 11(1): 4979. https://doi.org/10.1038/s41467-020-18734-9

[18] Dasgupta P, Kulkarni P, Majid S, Shahryari V, Hashimoto Y, Bhat NS, *et al*. MicroRNA-203 Inhibits Long Noncoding RNA HOTAIR and Regulates Tumorigenesis through Epithelial-to-mesenchymal Transition Pathway in Renal Cell Carcinoma. Mol Cancer Ther 2018; 17(5): 1061-1069. https://doi.org/10.1158/1535-7163.MCT-17-0925

[19] Wang X, Li Y, Pan M, Lu T, Wang M, Wang Z, *et al*. CEACAM5 inhibits the lymphatic metastasis of head and neck squamous cell carcinoma by regulating epithelial-mesenchymal transition via inhibiting MDM2. Clin Sci (Lond) 2022; 136(22): 1691-1710. https://doi.org/10.1042/CS20220581

[20] Tacutu R, Thornton D, Johnson E, Budovsky A, Barardo D, Craig T, *et al*. Human Ageing Genomic Resources: new and updated databases. Nucleic Acids Res 2018; 46(D1): D1083-d1090. https://doi.org/10.1093/nar/gkx1042

[21] Zhang L, Xu H, Ma C, Zhang J, Zhao Y, Yang X, *et al*. Upregulation of deubiquitinase PSMD14 in lung adenocarcinoma (LUAD) and its prognostic significance. J Cancer 2020; 11(10): 2962-2971. https://doi.org/10.7150/jca.39539

[22] Verma R, Aravind L, Oania R, McDonald WH, Yates JR, 3rd, Koonin EV, *et al*. Role of Rpn11 metalloprotease in deubiquitination and degradation by the 26S proteasome. Science 2002; 298(5593): 611-615. https://doi.org/10.1126/science.1075898

[23] Nardone C, Gao J, Seo HS, Mintseris J, Ort L, Yip MCJ, *et al*. Structural basis for the midnolin-proteasome pathway and its role in suppressing myeloma. Mol Cell 2025; 85(13): 2597-2609.e2511. https://doi.org/10.1016/j.molcel.2025.05.030

[24] Schnoell J, Scheiflinger A, Al-Gboore S, Kadletz-Wanke L, Kenner L, Heiduschka G, *et al*. The prognostic role of PSMD14 in head and neck squamous cell carcinoma. J Cancer Res Clin Oncol 2022. https://doi.org/10.1007/s00432-022-04072-4

[25] Lei J, Liu X, Liu W, Zhang Y, Liu Z. The prognostic value of USP14 and PSMD14 expression in non-small cell lung cancer. Ann Transl Med 2021; 9(12): 1019. https://doi.org/10.21037/atm-21-2748

[26] Jing C, Li X, Zhou M, Zhang S, Lai Q, Liu D, *et al*. The PSMD14 inhibitor Thiolutin as a novel therapeutic approach for esophageal squamous cell carcinoma through facilitating SNAIL degradation. Theranostics 2021; 11(12): 5847-5862. https://doi.org/10.7150/thno.46109

[27] Li J, Li Y, Xu F, Sun B, Yang L, Wang H. Deubiquitinating enzyme PSMD14 facilitates gastric carcinogenesis through stabilizing PTBP1. Exp Cell Res 2022; 415(2): 113148. https://doi.org/10.1016/j.yexcr.2022.113148

[28] Lee HJ, Lee DM, Seo MJ, Kang HC, Kwon SK, Choi KS. PSMD14 Targeting Triggers Paraptosis in Breast Cancer Cells by Inducing Proteasome Inhibition and Ca(2+) Imbalance. Int J Mol Sci 2022; 23(5). https://doi.org/10.3390/ijms23052648

[29] Sun T, Liu Z, Bi F, Yang Q. Deubiquitinase PSMD14 promotes ovarian cancer progression by decreasing enzymatic activity of PKM2. Mol Oncol 2021; 15(12): 3639-3658. https://doi.org/10.1002/1878-0261.13076

[30] Jing C, Duan Y, Zhou M, Yue K, Zhuo S, Li X, *et al*. Blockade of deubiquitinating enzyme PSMD14 overcomes chemoresistance in head and neck squamous cell carcinoma by antagonizing E2F1/Akt/SOX2-mediated stemness. Theranostics 2021; 11(6): 2655-2669. https://doi.org/10.7150/thno.48375

[31] Lv J, Zhang S, Wu H, Lu J, Lu Y, Wang F, *et al*. Deubiquitinase PSMD14 enhances hepatocellular carcinoma growth and metastasis by stabilizing GRB2. Cancer Lett 2020; 469: 22-34. https://doi.org/10.1016/j.canlet.2019.10.025

[32] Zhu R, Liu Y, Zhou H, Li L, Li Y, Ding F, *et al*. Deubiquitinating enzyme PSMD14 promotes tumor metastasis through stabilizing SNAIL in human esophageal squamous cell carcinoma. Cancer Lett 2018; 418: 125-134. https://doi.org/10.1016/j.canlet.2018.01.025

[33] Zhao X, Li M, Fu Y, Chen C, Chen Y, Xu L, *et al*. PSMD14-mediated PFKFB2 deubiquitination activates H3K27 lactylation to drive cancer stemness in gastric adenocarcinoma. Cell Death Differ 2025. https://doi.org/10.1038/s41418-025-01605-5

[34] Zhang W, Rong G, Gu J, Fan C, Guo T, Jiang T, *et al*. Nicotinamide N-methyltransferase ameliorates renal fibrosis by its metabolite 1-methylnicotinamide inhibiting the TGF-β1/Smad3 pathway. FASEB J 2022; 36(3): e22084. https://doi.org/10.1096/fj.202100913RRR

[35] Courtois L, Pinton A, Cabannes-Hamy A, Simonin M, Andrieu GP, Queri M, *et al*. Surface pTα expression predicts LCK activation and preclinical synergy of LCK and JAK coinhibition in adult T-ALL. Blood 2025; 145(24): 2903-2913. https://doi.org/10.1182/blood.2024027982

[36] Zhou J, Zhang Q, Guan J, Peng X, Lu Z, Zhou Q, *et al*. Computational and Experimental Investigation of Antidiabetic

Drugs on Tofacitinib Metabolism: Molecular Docking, in vitro, and in vivo Studies. Drug Des Devel Ther 2025; 19: 3845-3856. https://doi.org/10.2147/DDDT.S507141

[37] Nordmann TM, Anderton H, Hasegawa A, Schweizer L, Zhang P, Stadler PC, *et al*. Spatial proteomics identifies JAKi as treatment for a lethal skin disease. Nature 2024; 635(8040): 1001-1009. https://doi.org/10.1038/s41586-024-08061-0

[38] Avelar RA, Ortega JG, Tacutu R, Tyler EJ, Bennett D, Binetti P, *et al*. A multidimensional systems biology analysis of cellular senescence in aging and disease. Genome Biol 2020; 21(1): 91. https://doi.org/10.1186/s13059-020-01990-9

[39] Ogrodnik M, Miwa S, Tchkonia T, Tiniakos D, Wilson CL, Lahat A, *et al*. Cellular senescence drives age-dependent hepatic steatosis. Nat Commun 2017; 8: 15691. https://doi.org/10.1038/ncomms15691

[40] Wilkinson HN, Hardman MJ. Senescence in Wound Repair: Emerging Strategies to Target Chronic Healing Wounds. Front Cell Dev Biol 2020; 8: 773. https://doi.org/10.3389/fcell.2020.00773

[41] Lin W, Wang X, Wang Z, Shao F, Yang Y, Cao Z, *et al*. Comprehensive Analysis Uncovers Prognostic and Immunogenic Characteristics of Cellular Senescence for Lung Adenocarcinoma. Front Cell Dev Biol 2021; 9: 780461. https://doi.org/10.3389/fcell.2021.780461

[42] Zhang J, Gu J. Metabolic basis of fatty acid oxidation and immunotherapy resistance with clinical perspectives. Drug Resist Updat 2026; 84: 101317. https://doi.org/10.1016/j.drup.2025.101317

[43] Zhang J, Gu J, Zhang T, Xia R, Li J, Tan M, *et al*. The role of the aging process and related factor EMP1 in promoting progression of resectable pancreatic cancer. Genes Dis 2025; 12(5): 101490. https://doi.org/10.1016/j.gendis.2024.101490

[44] Gu J, Zhang J, Zeng S, Zhang W, Xia R, Wang X, *et al*. Artificial intelligence in tumor drug resistance: Mechanisms and treatment prospects. Intelligent Oncology 2025; 1(2): 73-88. https://doi.org/10.1016/j.intonc.2025.02.001

[45] Gu J, Zhang J, Xia R, Wang X, Yang J, Xie F, *et al*. The role of histone H1.2 in pancreatic cancer metastasis and chemoresistance. Drug Resist Updat 2024; 73: 101027. https://doi.org/10.1016/j.drup.2023.101027

[46] Gu J, Huang W, Wang X, Zhang J, Tao T, Zheng Y, *et al*. Hsa-miR-3178/RhoB/PI3K/Akt, a novel signaling pathway regulates ABC transporters to reverse gemcitabine resistance in pancreatic cancer. Mol Cancer 2022; 21(1): 112. https://doi.org/10.1186/s12943-022-01587-9

[47] Hanahan D. Hallmarks of cancer-Then and now, and beyond. Cell 2026. https://doi.org/10.1016/j.cell.2025.12.049

[48] Gu J, Huang W, Zhang J, Wang X, Tao T, Yang L, *et al*. TMPRSS4 Promotes Cell Proliferation and Inhibits Apoptosis in Pancreatic Ductal Adenocarcinoma by Activating ERK1/2 Signaling Pathway. Front Oncol 2021; 11: 628353. https://doi.org/10.3389/fonc.2021.628353

[49] Shukla S, Chen ZS, Ambudkar SV. Tyrosine kinase inhibitors as modulators of ABC transporter-mediated drug resistance. Drug Resist Updat 2012; 15(1-2): 70-80. https://doi.org/10.1016/j.drup.2012.01.005

[50] Huang Y, Wang Y, Zhang W, Wang W, Du L, Zhang X, *et al*. A Metastasis-Competent CAF Subpopulation Defined by $MFAP5^{7}THY1^{7}$ Co-expression Drives Prostate Cancer Metastasis via EMT Activation. Recent Pat Anticancer Drug Discov 2025. https://doi.org/10.2174/0115748928439833251118072935

[51] Li W, Ma X, Mei Y, Peng C, Feng Z. Aucubin Inhibits Liver Cancer via HMGB1-mediated Inactivation of the PI3K/AKT/mTOR Signaling Pathway. Recent Pat Anticancer Drug Discov 2025. https://doi.org/10.2174/0115748928420661250922102242

[52] Yang R, Feng H, Li S, Xu S, Wang Q, Wang H, *et al*. ZNF146-Mediated HMGB1-NF-κB Signaling Activation as a Therapeutic Target and Prognostic Biomarker in Osteosarcoma. Recent Pat Anticancer Drug Discov 2025. https://doi.org/10.2174/0115748928387577251118114459

[53] Chen Y, Mi Y, Tan S, Chen Y, Liu S, Lin S, *et al*. CEA-induced PI3K/AKT pathway activation through the binding of CEA to KRT1 contributes to oxaliplatin resistance in gastric cancer. Drug Resist Updat 2025; 78: 101179. https://doi.org/10.1016/j.drup.2024.101179

[54] Wang C, Zhong Y, Xu S, Cai W, Zhao J, Mao J, *et al*. TRIM24 promotes T-cell lymphoma development and glucocorticoid resistance via FUS-mediated phase separation of the glucocorticoid receptor. Drug Resist Updat 2025; 82: 101270. https://doi.org/10.1016/j.drup.2025.101270

[55] Zhang J, Gu J, Wang X, Xia R, Yang J, Gao M, *et al*. SLC6A14-mediated carnitine transmembrane uptake from PPARγ+ cancer-associated fibroblasts promotes recurrence of pancreatic cancer. Gut 2026; gutjnl-2025-336116. https://doi.org/10.1136/gutjnl-2025-336116

[56] Luo G, Hu N, Xia X, Zhou J, Ye C. RPN11 deubiquitinase promotes proliferation and migration of breast cancer cells. Mol Med Rep 2017; 16(1): 331-338. https://doi.org/10.3892/mmr.2017.6587

[57] Bharadwaj U, Kasembeli MM, Robinson P, Tweardy DJ. Targeting Janus Kinases and Signal Transducer and Activator of Transcription 3 to Treat Inflammation, Fibrosis, and Cancer: Rationale, Progress, and Caution. Pharmacol Rev 2020; 72(2): 486-526. https://doi.org/10.1124/pr.119.018440

[58] Huang HF, Murphy TF, Shu P, Barton AB, Barton BE. Stable expression of constitutively-activated STAT3 in benign prostatic epithelial cells changes their phenotype to that resembling malignant cells. Mol Cancer 2005; 4(1): 2. https://doi.org/10.1186/1476-4598-4-2

[59] Wang B, Xu X, Yang Z, Zhang L, Liu Y, Ma A, *et al*. POH1 contributes to hyperactivation of TGF-β signaling and facilitates hepatocellular carcinoma metastasis through deubiquitinating TGF-β receptors and caveolin-1. EBioMedicine 2019; 41: 320-332. https://doi.org/10.1016/j.ebiom.2019.01.058

Received on 07-02-2026 Accepted on 03-03-2026 Published on 25-03-2026

https://doi.org/10.30683/1929-2279.2026.15.08